Structural Features and Light-Dependent Changes in the Cytoplasmic Interhelical E−F Loop Region of Rhodopsin: A Site-Directed Spin-Labeling Study[†]

Christian Altenbach,[‡] Ke Yang,[§,||] David L. Farrens,[§] Zohreh T. Farahbakhsh,[‡] H. Gobind Khorana,[*,§] and Wayne L. Hubbell[*,‡]

Jules Stein Eye Institute and the Department of Chemistry & Biochemistry, University of California, Los Angeles, California 90095-7008, and Department of Biology and Chemistry, Massachusetts Institute of Technology, Cambridge, Massachusetts 02139

Received April 9, 1996; Revised Manuscript Received June 17, 1996[⊗]

ABSTRACT: Thirty consecutive single cysteine substitution mutants in the amino acids Q225−I256 of bovine rhodopsin have been prepared and modified with a sulfhydryl specific nitroxide reagent. This sequence includes the E−F interhelical loop, a transducin interaction site. The accessibilities of the attached nitroxides to collisions with hydrophilic and hydrophobic paramagnetic probes in solution were determined, and the electron paramagnetic resonance spectra analyzed in terms of side chain mobility, both in the dark and after photoactivation. Accessibility data shows that the rhodopsin polypeptide chain crosses an aqueous/hydrophobic boundary in the range V227−K231 and again in the range V250−V254. In the hydrophobic segments, both the accessibility and mobility data are consistent with helical structures. In the regions of the sequence located within the aqueous phase, periodic variation in both accessibility and mobility of the spin-labeled side chains indicates that the E−F interhelical loop is largely α-helical, being formed by regular extensions of the E and F helices by about 1.5 and 3 turns, respectively. Judging from nitroxide mobilities, the putative extension of helix E in the aqueous phase is more dynamic than that of helix F. Changes in the electron paramagnetic resonance characteristics of the spin-labeled rhodopsin upon photoactivation indicate that chromophore isomerization results in patterns of structural changes that can be interpreted in terms of movements of helices that extend into the aqueous loop regions.

Rhodopsin is the membrane-bound photoreceptor protein of the vertebrate rod cell. Upon photoactivation, rhodopsin undergoes a conformational change of unknown nature at the cytoplasmic surface that leads to activation of the visual G protein transducin (Konig et al., 1989). Rhodopsin contains 348 amino acids, and compelling biophysical and biochemical data indicate that it consists of seven transmembrane α-helices. Hydropathy considerations and results from site-directed spin−labeling experiments in helices C and D (Farahbakhsh et al., 1995) suggest that the polypeptide intersects the membrane/solution boundary approximately as indicated in the secondary structural model shown in Figure 1. On the basis of sequence comparisons of 204 members of the G-coupled receptor family, Baldwin proposed a packing arrangement of the helices (Baldwin, 1993). Recently, low-resolution structural models of frog and bovine rhodopsin have been derived from electron diffraction data from two-dimensional crystals (Schertler et al., 1993; Unger & Schertler 1995; Schertler & Hargrave, 1995). Four relatively straight transmembrane helices are resolved, with three others presumed to be tilted with respect to the others. The model is generally consistent with the packing arrangement proposed by Baldwin.

While the general motif of the rhodopsin molecule appears to be clear, specific structural information, particularly in the interhelical loop regions involved in transducin activation, is lacking. In addition, the mechanism whereby the isomerization of retinal leads to exposure of transducin interaction sites remains to be understood in structural terms. An attractive model for the propagation of structural changes from the site of retinal to the interhelical loops is rigid body movements of the α-helices, a mechanism with precedent in water-soluble proteins (Gerstein et al., 1994) and apparently in bacteriorhodopsin (Subramaniam & Henderson, 1994; Steinhoff et al., 1994).

The technique of site-directed spin-labeling has proven to be useful for the investigation of structure and function in membrane proteins [see Hubbell and Altenbach (1994) for a recent review]. The experimental approach has been to introduce single reactive cysteine residues in the protein to provide attachment sites for nitroxide spin−labels. Analysis of the EPR[1] spectra and accessibilities of the attached nitroxides to collision with paramagnetic reagents in solution has been used to identify secondary structure (Altenbach et al., 1990), map topography (Todd et al., 1989; Greenhalgh et al., 1991; Resek et al., 1993; Zhan et al., 1995), determine the depth of immersion of residues on the outer surface of a transmembrane helix (Altenbach et al., 1994), and time-resolve conformational changes (Shin et al., 1993; Farahbakhsh et al., 1993; Steinhoff et al., 1994).

[†] Research reported here was supported by NIH Grants EY05216 (W.L.H.) and GM28289 (H.G.K.), NIH National Research Service Award EY06465 (D.L.F.), and the Jules Stein Professorship endowment. This is paper 18 in the series "Structure and Function in Rhodopsin"; paper 17 is Yang et *al*., 1996).

* To whom correspondence should be addressed.

[‡] Jules Stein Eye Institute, UCLA.

[§] Massachusetts Institute of Technology.

[||] Present address: Memorial Sloan-Kettering Cancer Center, 1275 York Avenue, New York, NY 10021.

[⊗] Abstract published in *Advance ACS Abstracts,* September 1, 1996.

[1] Abbreviations: DM, dodecyl maltoside; DPPH, 2,2-diphenyl-1-picrylhydrazyl; EPR, electron paramagnetic resonance; NiAA, nickel (acetylacetonate)$_2$; NiEDDA, nickel ethylenediamine diacetate.

S0006-2960(96)00849-5 CCC: $12.00

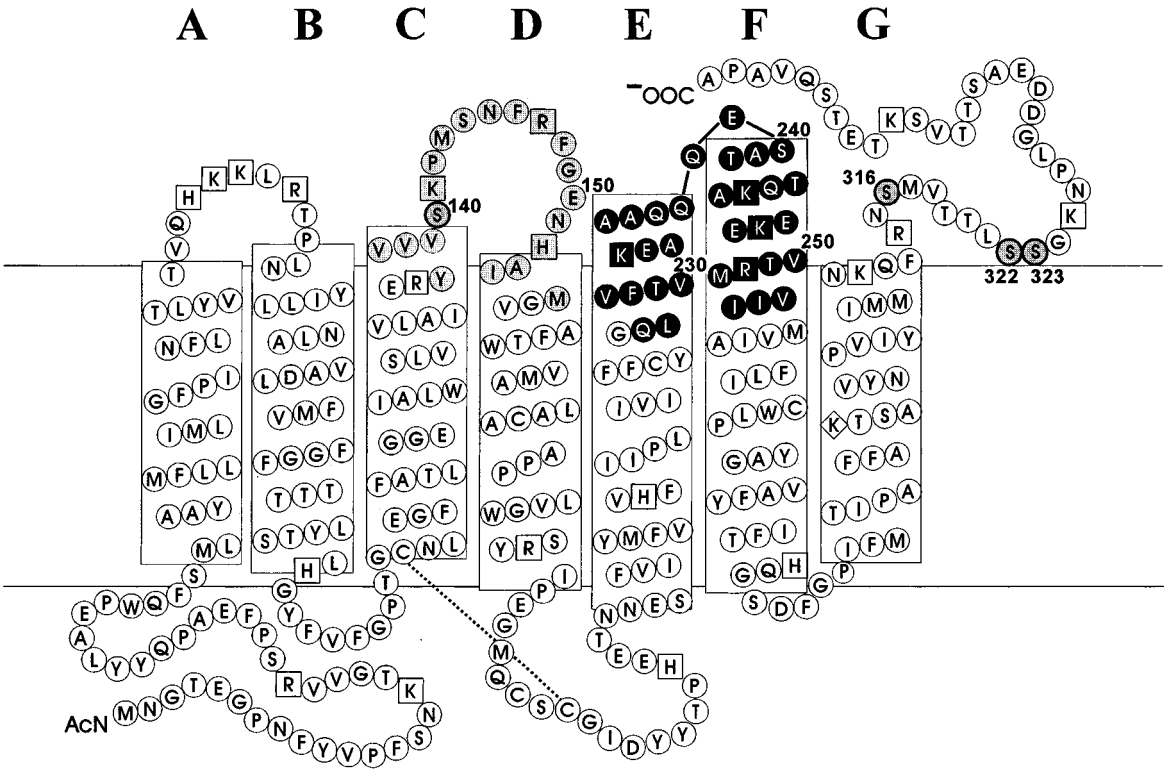

FIGURE 1: Secondary structural model of rhodopsin. The sites included in this study, 225−256, are indicated in black. Sites included in a previous study, 136−155 (Farahbakhsh et al., 1995), are shaded. The positions of the native cysteine residues replaced by serine are circled. The horizontal lines define the approximate boundaries of the phospholipid bilayer.

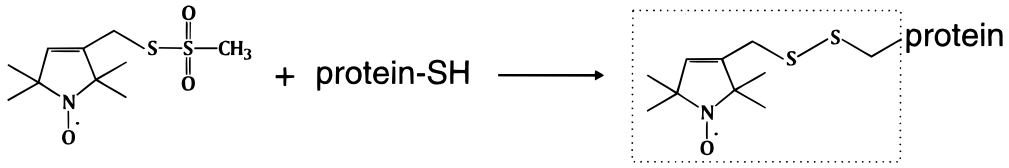

FIGURE 2: Reaction of spin-label **I** to generate the nitroxide side chain **R1**.

In a previous study, nitroxide scanning mutagenesis was employed to map topology and light-dependent structural changes in the C−D interhelical loop region of bovine rhodopsin (Farahbakhsh et al., 1995). It was concluded that the topology of sites in the C and D helices were compatible with predictions derived from electron diffraction (Schertler et al., 1993). Light-induced changes in structure were identified and interpreted in terms of rigid body motion of the C helix.

The present study extends this line of investigation with thirty single cysteine substitution mutants of rhodopsin in the amino acids Q225−I256, which include the putative E−F interhelical loop (see Figure 1). The results localize the aqueous/hydrophobic boundaries of the E and F helices, suggest that these helices extend beyond the membrane surface into the aqueous medium, and map light-dependent structural changes in this region of the molecule.

EXPERIMENTAL PROCEDURES

Spin-Labeling and EPR Spectroscopy of Rhodopsin Mutants

Single cysteine substitutions were prepared and purified as described in the companion paper (Yang et al., 1995). Spin-labeling was carried out as previously described (Resek et al., 1993).

Reaction of the spin-label **I** with cysteine produces a new side chain containing a disulfide-linked nitroxide, which will be referred to as **R1** (see Figure 2). The various spin-labeled substitution mutants are designated by giving the original residue, the amino acid number, and the new residue. For example, Q225R1 denotes a mutant in which the native glutamine at position 225 is replaced by the spin-labeled amino acid R1.

Solutions of spin-labeled rhodopsin mutants (typically 60 μg in 1 mL) were concentrated to a final volume of 10−20 μL using filtration units (Millipore Ultrafree-MC, 10 000 MW cutoff). This step also results in concentration of DM. This is in fact advantageous, since it has previously been shown that rhodopsin thermal stability increases with increasing concentration of DM up to at least 200 mM (Knudsen & Hubbell, 1978), well above the maximum concentrations achieved during the concentration procedure.

Samples of ≈2 μL were loaded in TPX capillaries (Jagmar, Poland), and the EPR spectra were recorded at 19−21 °C under field-frequency lock with a Varian E-109 spectrometer operating at X-band and fitted with a loop−gap resonator (Hubbell et al., 1987). The microwave power was 2 mW incident, and the modulation amplitude was optimized to avoid spectral distortion (≤2 G). Signal-averaged spectra (4−8 scans) were obtained with a 100 G sweep at 30 s/scan using a Nicolet 1280 computer. Spectra were recorded both in the dark and after 1 min of photobleaching with a fiber optic illuminator (Cole Parmer, Chicago, IL) equipped with a long-wavelength pass filter (Melles-Griot, $\lambda \geq 500$ nm) and an infrared filter. Previous studies indicated that the

majority of the pigment was in the MII state under the conditions described (Resek et al., 1993).

Power saturation measurements for the spin-labels attached to rhodopsin were carried out under N_2, in the presence of O_2 in equilibrium with air and with 20 mM NiEDDA, and the data were analyzed in terms of the parameter $P_{1/2}$ (Altenbach et al., 1989). The quantity $\Delta P_{1/2}(R) = P_{1/2}(R) - P_{1/2}(N_2)$ is proportional to the collision frequency of the protein-bound nitroxide with a paramagnetic reagent R, but also depends on spectrometer performance and T_{2e} of the nitroxide. A more useful quantity to measure collision rate is Π, the "accessibility parameter":

$$\Pi = \frac{\Delta P_{1/2}(R)}{P_{1/2}(DPPH)} \frac{\Delta H(DPPH)}{\Delta H}$$

where $P_{1/2}$(DPPH) is $P_{1/2}$ for a DPPH crystal, ΔH(DPPH) is the peak-to-peak line width of the DPPH resonance, and ΔH is the corresponding line width of the nitroxide central resonance (Farahbakhsh et al., 1992). The accessibility parameter normalizes both spectrometer performance and T_{2e} effects and is ideally a pure measure of collision frequency.

RESULTS

*Reaction of Mutants with Spin-Label **I** and EPR Spectra*

The single cysteine mutants were all prepared from a "base" mutant in which the native cysteines C140, C316, C322, and C323 were replaced by serines but which contained the native cysteines C110, C167, C185, C187, C222, and C264. Cysteines C110 and C187 form a disulfide bond (Karnic & Khorana, 1990) and are unreactive to spin-label **I**, as is C185 under the conditions employed here (Farahbakhsh et al., 1995). Spin-labeling of the base mutant gives a weak background EPR signal due to limited reaction of **I** with the remaining sulfhydryls (Figure 3), corresponding to less than 0.3 spins/rhodopsin (Resek et al., 1993).

All of the single cysteine substitution mutants in the series 225−256 except 229 and 254 reacted with **I** in the dark (ground state) to give the EPR spectra shown in Figure 3 (solid lines). The EPR spectral amplitudes of the labeled cysteine mutants are considerably greater than that from the base mutant, and each has a unique spectral line shape. This supports the conclusion that the spectra arise predominately from spin-labels attached to the introduced cysteines rather than the background cysteines of the base mutant. In addition, the EPR spectra of R1 at most of the sites change upon rhodopsin photoactivation, unlike that of the base mutant.

Although quantitative determination of the extent of modification was not carried out, previous studies of the reaction of **I** with several single cysteine mutants in the cytoplasmic domain of rhodopsin in DM showed that modification was essentially complete under the reaction conditions employed here (Resek et al., 1993). However, the relatively low signal-to-noise in the EPR spectra from residues 228 and 253 suggests incomplete modification at these sites. It is interesting to note that these residues are adjacent in sequence to the two unreactive cysteines, 229 and 254.

UV/Vis Absorption Spectra of the Spin-Labeled Mutants

The UV/vis absorption spectra for all of the spin-labeled mutants were similar, with absorption maxima of 500 ± 1 nm and spectral ratios A_{280}/A_{500} of 1.6−1.8, essentially identical to the wild type protein.

Topography in the Sequence 225−256

In this study, rhodopsin is solubilized in the DM micelle. Information on the topographical location of a nitroxide side chain relative to the aqueous/hydrophobic boundary in the micelle can be obtained by determining the collision rate of the nitroxide with paramagnetic reagents of polar ($\mathbf{R_p}$) and nonpolar ($\mathbf{R_{np}}$) character. For this purpose, it is convenient to define the function $\Phi = \ln\{\Delta P_{1/2}(\mathbf{R_{np}})/\Delta P_{1/2}(\mathbf{R_p})\}$, where $\Delta P_{1/2}$ is an experimental quantity proportional to the collision rate of the reagent with the protein-bound nitroxide (Altenbach et al., 1994). The value of $\Delta P_{1/2}$ for any reagent depends on the protein structure around the nitroxide, the diffusion coefficient, and local concentration of reagent. However, Φ itself is not strongly dependent on protein structure, since steric factors involved in the collision event approximately cancel in forming the ratio of $\Delta P_{1/2}$ values for two different reagents, assuming that they are of similar size. The parameter Φ is expected to be approximately constant for nitroxides exposed to the aqueous medium, but to increase upon entering a hydrophobic region due to the higher solubility of $\mathbf{R_{np}}$ compared to $\mathbf{R_p}$. Using NiAA and O_2 as the polar and nonpolar reagents, respectively, Altenbach et al. (1994) found Φ to be a linear function of the depth of bilayer immersion for nitroxide side chains located on the bacteriorhodopsin transmembrane helix D. Similar results were reported for NiEDDA as the polar reagent.

In previous studies on rhodopsin in DM micelles, Φ was used with NiEDDA and O_2 as reagents to locate the sequence where the rhodopsin polypeptide enters the hydrophobic micelle interior (Farahbakhsh et al., 1995). In that study, phospholipids with a spin-label in the polar head group and at various points along a hydrocarbon chain were solubilized in DM micelles and used to calibrate Φ for these reagents. For 20 mM NiEDDA and O_2 in equilibrium with air, it was found that nitroxides in the polar headgroup region have $\Phi \approx 0$, defining the outer boundary of the interface. Due to the size difference between NiEDDA and O_2, Φ cannot be quantitatively analyzed at sites where local steric constraints are extreme, since this would result in a size exclusion of NiEDDA relative to the smaller O_2. Fortunately, this situation is readily recognized by immobilization of the nitroxide, and such points are excluded from analysis.

Because the range of values of Φ is small through the micelle interface, it is useful to employ the simple ratio of $\Delta P_{1/2}$ values, e^{Φ}, rather than its logarithm for purposes of graphical presentation. Figure 4 shows a plot of e^{Φ} *versus* amino acid number in the series 225−256. Sites 226, 230, 243, 244, and 247−251 have been excluded from the plot since they have relatively immobilized nitroxide EPR spectra, and Φ may be influenced by steric exclusion effects as mentioned above. Taking $e^{\Phi} = 1$ ($\Phi = 0$) as the outer limit of the aqueous/hydrophobic boundary, it can be seen that the polypeptide crosses the boundary in the range V227−K231 and again in the range V250−I254. This assignment corresponds to changes in slope in the plot, as would be expected.

Structure in the Sequence 225−256

While the ratio $\Delta P_{1/2}(O_2)/\Delta P_{1/2}$(NiEDDA) reveals features of the local solvent polarity, the accessibility parameter,

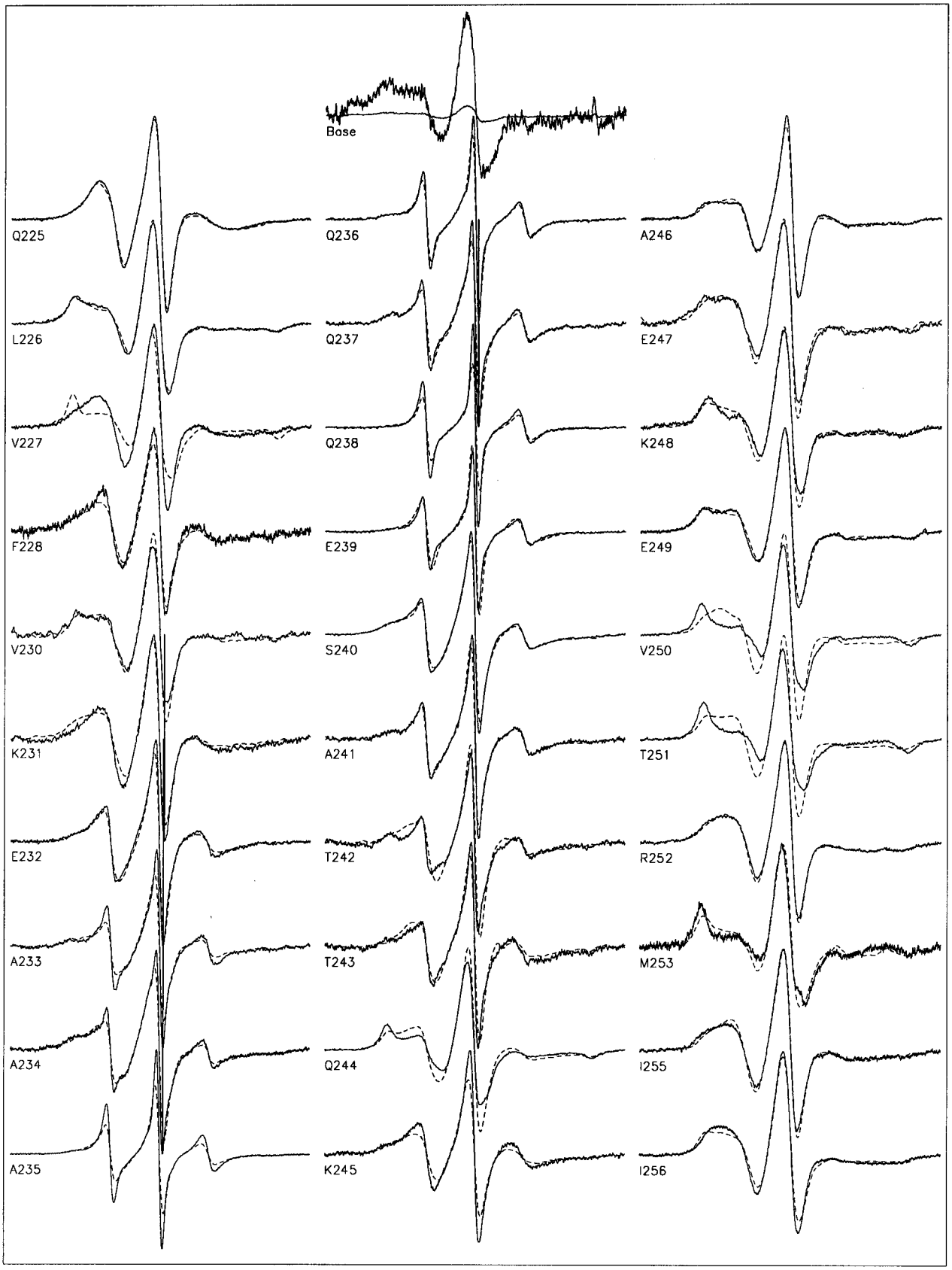

FIGURE 3: Room temperature EPR spectra of the spin-labeled mutants in the dark (solid trace) and after photoactivation (dotted trace). The spectra from photoactivated rhodopsin were digitally filtered to remove high-frequency noise so that the dotted trace is distinguishable from the solid. The original noise level was the same as for the dark spectra. The noisy trace for the base mutant background signal is normalized to approximately the same amplitude as the other spectra to reveal the line shape. The superposed low-amplitude trace is the approximate signal size on a scale similar to the other spectra.

Π , and the mobility of the nitroxide side chain contains information on the protein structure. The term "mobility" is used in a general sense and includes effects due to motional rate, amplitude, and geometry. Accessibility data for protein domains in a homogeneous phase are relatively simple to interpret in terms of local structure: the higher the density of neighboring residues around the nitroxide, the lower the accessibility. Thus residues in the protein interior will have

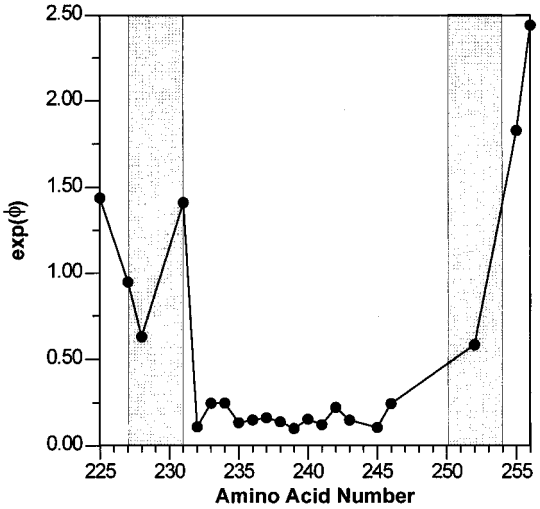

FIGURE 4: A plot of e^{Φ} *versus* amino acid number. Missing data points are those having immobilized line shapes, and thus which are not valid for analysis, or to sites that could not be labeled (229, 254). The shaded zones mark the apparent aqueous/hydrophobic boundary regions.

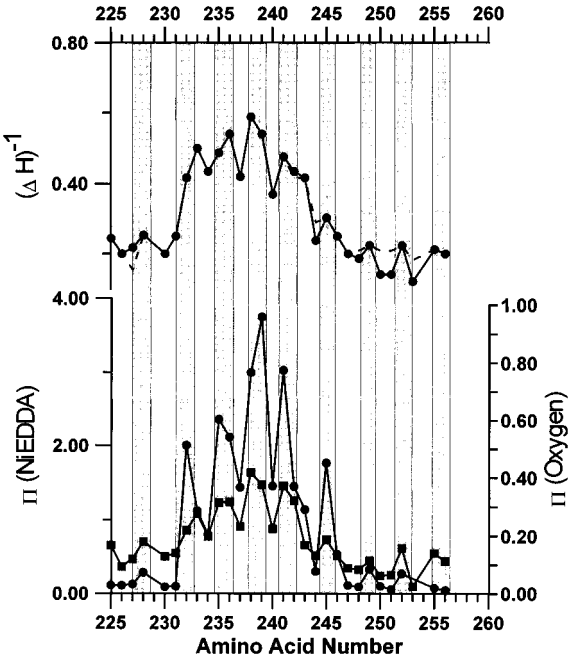

FIGURE 5: Π(NiEDDA) (●, bottom), Π(O_2) (■, bottom), and the reciprocal of the central line width, ΔH^{-1} (●, top) *versus* amino acid number in the dark state. The dashed line indicates ΔH^{-1} after bleaching. Missing data points (229, 254) are sites that could not be modified with spin-label **I**. The shaded zones highlight the residues having local maxima in the Π values.

low accessibilities compared to those on water or lipid-exposed surfaces. Nitroxide scanning mutagenesis through a sequence of regular secondary structure will in general reveal periodic variations in accessibility that can serve to identify the type of secondary structure and its orientation in the protein. This was first demonstrated for residues in the transmembrane E helix of bacteriorhodopsin using Π(O_2) (Altenbach et al., 1990).

The mobility of a nitroxide side chain reflects structure in part through direct steric interaction. Residues with extensive tertiary contacts interactions, such as those in the protein interior, are immobilized on the time scale of protein rotational diffusion. Exposed surface residues have a high mobility with effective rotational correlation times in the 1−3 ns range (Altenbach et al., 1994a). Mobility, like accessibility, is periodic in a nitroxide scanning experiment through regular secondary structure (Hubbell & Altenbach, 1994b). In addition, the mobility of a nitroxide side chain provides insight into the dynamics of the protein backbone (see Discussion). Information on nitroxide mobility is encoded in the EPR spectral line shapes, and a rigorous analysis requires spectral simulation techniques (Freed, 1976). For simplicity of graphical presentation, the reciprocal of the line width of the central ($m_I = 0$) resonance of the nitroxide will be taken as a crude but practical estimator of nitroxide mobility. The reciprocal of the line width is taken so that the quantity increases with increasing mobility.

Figure 5 shows Π(O_2), Π(NiEDDA) (lower panel), and the reciprocal line width (upper panel) for all residues investigated. The estimated experimental errors in the quantities are within the size of the data symbols. A striking oscillatory behavior of all three quantities is evident, unbroken, throughout the entire sequence. The amplitudes of the functions change sharply in the vicinity of the aqueous/hydrophobic boundaries. In the case of the Π values, this is due to changes in the solubility and diffusion constant for the paramagnetic reagents. In the case of the mobility, it is due to changes in the structural order of the protein (see Discussion). For convenience, the hydrophobic and aqueous segments of the sequence are considered separately below.

The sequences 225−231 and 250−256 correspond to the predicted hydrophobic domains and boundary regions at the cytoplasmic surface of the protein for helices E and F, respectively (Figures 1 and 4). A qualitative examination of both the reciprocal line widths and the EPR line shapes (Figure 3) reveal that R1 at residues 226, 230, 250, 251, and 253 are immobilized, characteristic of residues buried in the interior of a protein with strong tertiary interactions. R1 side chains at 225, 227, 228, 231, 252, 255, or 256 have higher mobility, similar to those on the outer surfaces of the transmembrane helices in bacteriorhodopsin (Altenbach et al., 1989; Hubbell & Altenbach, 1995). The accessibility parameter Π(O_2) closely follows the variations in reciprocal line width, i.e., they vary *in phase*, indicating that the most mobile sites are also the most accessible to collision. Thus the periodic behavior in the quantities arises from regular alternations of the side chains between buried and exposed sites in the structure, as observed earlier in a nitroxide scanning experiment in a transmembrane helix of bacteriorhodopsin (Altenbach et al., 1990). Similar conclusions follow from the values of Π(NiEDDA).

The sequence 232−249 is exposed to the aqueous medium (Figure 4). The obvious periodicity in all quantities in this region, made more pronounced by the large amplitude changes, clearly suggests that a regular secondary structure exits in this E−F interhelical loop domain. As in the hydrophobic segments, the oscillations in Π(O_2), Π(NiEDDA), and the reciprocal line width are *in phase* with one another, suggesting a regular alternation of the side chains, in sequence, between different environments in the local structure. However, the mobilities of the R1 side chains are much higher at all sites in the range 232−247 compared to those in the hydrophobic domains, as reflected in the reciprocal line width plot.

Structural Changes Associated with Photoactivation

Many of the sites show detectable changes in EPR spectral line shape, and hence mobility, upon photoactivation (Figure

3). Only the largest of the changes are detected by the reciprocal line width measure (Figure 5, upper panel, dotted line). Within the transmembrane and interfacial domain of helix E (225−231), a large change is observed only at site 227, representing an effective immobilization of the nitroxide. This is one of the largest changes observed, readily apparent in the reciprocal line width change, and can only arise from an increase in tertiary interaction at this site. A modest decrease in mobility is also noted from the line shape change at 231, which lies only 40° away from 227 on a helix surface. Minor decreases in the mobility apparent at other sites may arise from changes in backbone dynamics (see Discussion).

In the interfacial and transmembrane domain of helix F, large *increases* in mobility are seen at 250 and 251, with a smaller but significant increase at 253, indicating a decrease in tertiary interaction at these immobilized sites.

Changes due to photoactivation are also resolved throughout the regions of the sequence located in the aqueous phase with the largest change at 244. Possible interpretations of these changes will be discussed below.

DISCUSSION

Topography

The Φ data in Figure 4 indicate that the rhodopsin polypeptide crosses an aqueous/hydrophobic boundary twice in the sequence 225−256. The boundaries are not sharp but are zones involving a number of amino acids equivalent to about one turn of an α-helix. The diffuse nature of the boundary is not surprising considering that the protein is in a micelle rather than a phospholipid bilayer. The boundary zones identified (Figure 4) correspond reasonably well to those expected from hydropathy considerations (Figure 1).

The parameter Φ for a nitroxide is a function of distance within the hydrophobic interior of a bilayer due to spatial gradients in the concentrations of the paramagnetic reagents (Altenbach et al., 1994). It is expected that Φ should change continuously across the boundary zone and approach a constant value for nitroxides in the bulk aqueous phase. Figure 4 shows that residues within the sequence 232−245 have essentially constant Φ values even though individual Π values vary widely. The average value of Φ in this region is −1.75. Earlier Φ data for solvent-exposed residues in the C−D interhelical loop had an average value of $\Phi \approx -0.30$ (Farahbakhsh et al., 1995). The comparison suggests that the C−D loop residues are all closer to the interface than those in the E−F interhelical loop, consistent with the longer length of the latter loop and the proposed helical extensions.

Structure within the Transmembrane Domains of Helices E and F

Recently, Schertler and co-workers have constructed a low-resolution model for the packing of the rhodopsin transmembrane helices on the basis of electron crystallography (Schertler et al., 1993; Unger & Schertler, 1995; Schertler and Hargrave, 1995), and Baldwin has proposed a specific mapping of the rhodopsin sequence onto these helices (Baldwin, 1993). According to the topographical analysis of Figure 4, residues 225−231 and 250−256 correspond to segments of the intramembrane E and F helices near the cytoplasmic membrane boundaries (Figures 1 and 4). The data on accessibility and mobility for the R1 side chain in these sequences provide a direct means of mapping the residues on to helix packing models of rhodopsin.

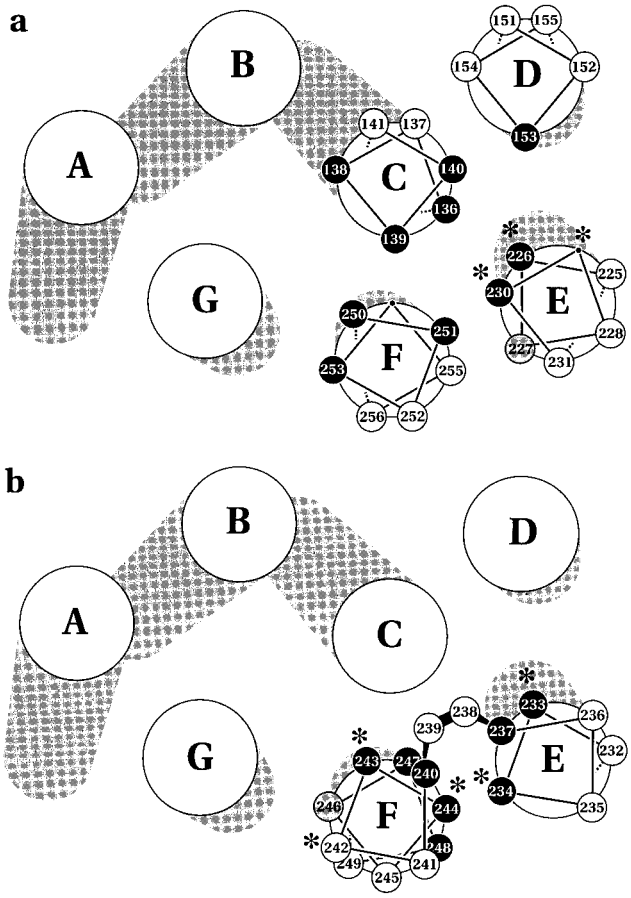

FIGURE 6: Packing model for the rhodopsin helices based on Unger and Schertler (1995) and Baldwin (1993) showing proposed locations of (a) residues 225−231 and 250−256, the hydrophobic segments, and (b) residues 232−249, the water-exposed segment. The solid symbols indicate sites which lie at or near *minima* in the Π and reciprocal line width functions of Figure 5. The open symbols are sites which lie at or near *maxima* of those functions and are predicted to be exposed on the protein surface. Shaded symbols identify residues at transitions between these regions. Data for helices C and D are from Farahbakhsh et al. (1995). The sites where cysteine substitution resulted in loss of ability to activate transducin are marked with asterisks (Yang et al, 1996).

Figure 6a shows a model for the rhodopsin transmembrane helices according to Unger and Schertler (1995) with the locations of the amino acids of the aforementioned sequences placed according to the data in Figure 5 and Farahbakhsh et al. (1995b). The solid symbols indicate sites which lie at or near *minima* in the $\Pi(O_2)$ and reciprocal line width functions of Figure 5. These sites have low accessibilities and mobilities and identify surfaces of strong tertiary interactions buried within the protein interior. The open symbols are sites which lie at or near *maxima* those functions and are predicted to be exposed on the protein surface. Shaded symbols identify residues at transitions between these regions. Included in the figure are residues from a recent study in helices C (136−141) and D (151−155) (Farahbakhsh et al., 1995). It is evident that the regular variations in the data from this and the earlier study are in excellent agreement with the model proposed by Baldwin (1993).

Structure in the Solvent-Exposed Sequence

Throughout the rhodopsin sequence exposed to the aqueous phase (232−249), in-phase periodic variations are noted

for $\Pi(O_2)$, Π(NiEDDA), and the reciprocal line width. Since the periodicity continues unbroken across the aqueous/hydrophobic boundary, it is natural to consider helical extensions of the E and F transmembrane segments into the aqueous phase as a simple model to explain the data. To examine this possibility, consider again the model in Figure 6. Figure 6b shows the sequence 232−249 mapped onto the model assuming regular helical extensions of E (232−237) and F (240−249) with an interconnecting turn formed from residues 238 and 239. The symbols have the same meaning as in Figure 6a. It is evident that the data are in reasonably good agreement with this model. However, the data suggest that residue 248 has more extensive tertiary contacts and less accessibility than implied by the model and *vice versa* for residue 246. The model could be brought into closer agreement with the data by a counterclockwise rotation of the F helix extension. Alternatively, slight rearrangements in the helical packing scheme would produce the same effect.

Although residue 249 is at a local maximum in accessibility and mobility, the absolute values of these parameters are unusually low for a residue expected to lie on the outer surface of a helix. This could result from a local irregularity in helix F or from tertiary interaction with some feature of the structure not represented in the model, namely the long solvent exposed C-terminal domain (312−350) extending from nearby helix G.

In the model of Figure 6b, the E helix is extended by about 1.5 turns and the F helix is extended by about 3 turns, with an interconnecting loop centered at residues 238−239. The relative lengths of the helices and the location of the turn are ambiguous, since the periodic data may be accommodated by another model in which residue 240 is the final residue in the extension of helix E rather than the first residue in the F helix extension as shown in Figure 6b. In this alternative, the interhelical turn would be composed of residues 241−243, and the E and F helical extensions would be of equal length. The model shown in the figure is preferred, since the very high mobilities and accessibilities of R1 at 238 and 239 are most easily accounted for in a turn. In addition, the papain and thermolysin cleavage sites in the E−F interhelical loop are located near these residues.

On the basis of an FTIR proteolysis study of rhodopsin in the native membrane, Pistorius and de Grip (1994) suggested the presence of helical structure in the E−F loop. More recently, Yeagle et al. (1995) reported the NMR determination of the solution structure of a 22 amino acid peptide corresponding to the E−F interhelical loop. The first six amino acids (N-terminal) produced insufficient constraints to determine a structure, while the last six amino acids (C-terminal) gave only modest constraints. The central region of the peptide did provide sufficient constraints to resolve a short helical segment. However, the conformation of the loop suggested in the model proposed by Yeagle et al. (1995) is significantly different than that reported here.

Side Chain Mobilities in the E and F Helices and the Interhelical Loop

Like the accessibilities, the mobilities of the nitroxide side chains also reflect local structure. The dynamics of the nitroxide side chain has contributions from the rotational motion of the protein as a whole, the motion of the side chain relative to the backbone, and the motion of the backbone relative to the average structure (Mchaourab et al., 1996). The rotational motion of the protein is too slow to materially influence the dynamics of most of the side chains discussed below, and the line shapes reflect the latter 2 degrees of freedom. In the motional narrowing regime where most of the spectra lie, spectral simulations are required to quantitatively analyze the motions (Freed, 1976). However, the reciprocal line width is an estimator that can provide a useful representation of local variations in mobility when employed together with qualitative features of the line shape. In the motional narrowing regime, this parameter reflects the degree of averaging of the g factor anisotropy, and will be sensitive to anisotropy of motion as well as motional rate and amplitude. Nevertheless, the parameter generally reflects a simple periodic behavior *in phase* with that of the Π values, and correlates with the accessibilities at all sites (Figures 5). The reciprocal peak-to-peak line width in the first-derivative EPR spectrum is a poor measure of average mobility in cases where the line shape clearly reveals two populations of very different mobility. In this situation, the more mobile component dominates the line width measurement, even though the components may be present in comparable amounts. Examples are the spectra of A233R1, A234R1, and T242R1, and the average mobility based on reciprocal line width is overestimated at these sites. This error is in a direction such that a correction would improve the agreement in periodicity between the reciprocal line width and Π values at these points.

R1 residues lying primarily in the putative E helical extension have EPR spectra that reflect a significantly higher mobility than those residues in the F helix. This is reflected in the asymmetry of the reciprocal line width data in Figure 5 about residues 238−239. Apparently, even residues predicted to lie at contact faces of the helix E extension are more mobile than those at the outer surface of helix F. Thus an additional degree of motional freedom is implied for these residues, presumably segmental motions of the backbone relative to the average protein structure. Thus we suggest that the putative E helix extension has a dynamic, or flexible, main chain relative to the F helix extension. It is not yet possible to estimate the amplitude of the fluctuations in the backbone since simulations of these complex spectra remain to be carried out, but the correlation time must be in the nanosecond range. One striking result is that residues 226, 229, 230, 233, 234, 242, 243, and 244, identified in the accompanying study as essential for transducin activation (Yang et al., 1995), all lie along the inward face of the E and F helices (Figure 6a and b, residues marked with "*"). The dynamic nature of the E helix suggests that this region of the protein is optimized for function rather than structure. Perhaps the flexibility of this helix is required to adopt an optimal conformation for the interaction, or to limit the binding constant of transducin through the loss in entropy of the loop that would be incurred upon binding.

The data in Figure 5 also reveals a general *gradient* of mobility in both the E and F helical extensions such that mobility is lowest in the transmembrane helical segments and increases with distance from the aqueous/hydrophobic boundaries. This is in accord with the greater strength of backbone hydrogen bonds in low dielectric media.

Site-directed spin-labeling experiments have been previously carried out in the sequence 136−155 which includes the C−D interhelical loop (Farahbakhsh et al., 1995). Mutants N151R1, H152R1, and M155R1 have EPR spectra

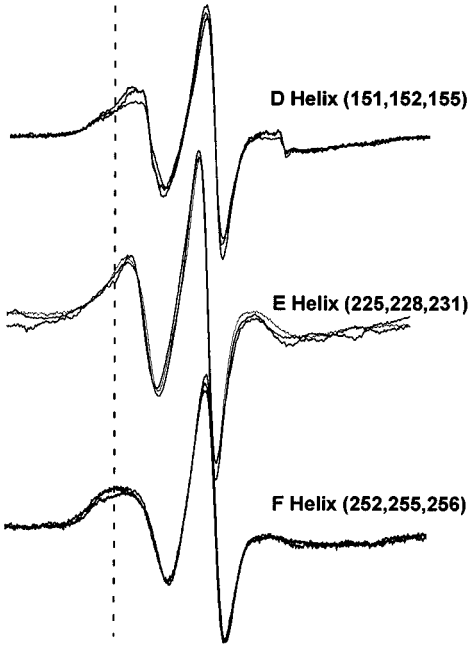

FIGURE 7: EPR spectra of **R1** residues located on the outer surface of transmembrane helices in rhodopsin.

and accessibilities consistent with their location on the surface of the D helix facing the hydrophobic interior of the DM micelle, in agreement with the model of Figure 6. The EPR spectra of spin-labels at these positions together with spectra from similarly located residues in the E and F helices are shown in Figure 7. The similarity of the line shapes for residues on the outer surface of a given helix is remarkable, suggesting that the mobilities of these residues are not primarily determined by interactions with nearest-neighbor side chains in the same helix, since the sequence is different at all sites. Although the spectra within the same helix are similar, they are distinctly different between different helices. The data in Figure 7 indicate the highest mobility for the R1 residues at the outer face of helix E, and the lowest in helix F, as judged by the line widths and relative breadth of the spectral features. These may reflect differences in helix internal fluctuations, which would suggest that the higher mobility of the E helix extension discussed above extends into the transmembrane helical domain.

For nitroxides in the slow motional regime with well-resolved outer hyperfine extrema, the separation of the outer hyperfine extrema ($2A_{zz}$) may be taken as an simple and quantitative measure of mobility (Goldman et al., 1972). The nitroxides located at 226, 230, 244, 247, 248, 249, 250, 251, and 253 are in this category, and with the possible exception of residues 248 and 249, they are predicted to be buried in the protein interior or at contact surfaces between helices. The longest correlation time, ~40 ns, is found for M253R1. This is a lower limit to the correlation time of the protein−detergent complex, which corresponds to a molecular weight of about 140 kD, assuming a Stokes−Einstein spherical particle.

Structural Changes Associated with Photoactivation

In the DM micelle, photoactivation produces the MII state that decays with release of retinal with a half-time of approximately 15 min in 0.1% DM at 20 °C (Farrens & Khorana, 1995). In the present experiments, rhodopsin is bleached for 1 min, and the spectrum recorded within 2 min.

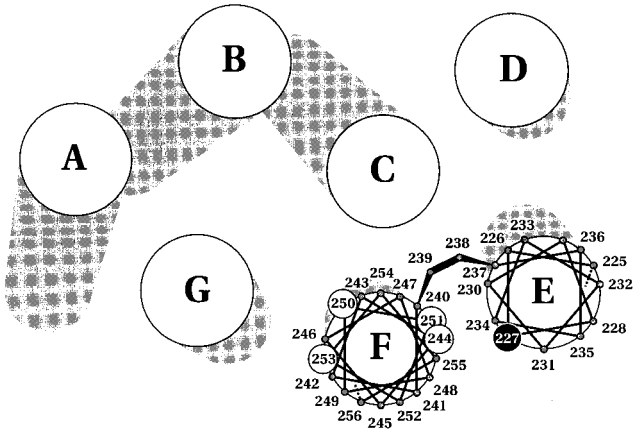

FIGURE 8: Rhodopsin model of Figure 7 showing sites of the largest changes in mobility produced by photoactivation. Solid and open symbols indicate decrease and increase in mobility, respectively.

Thus we assume that the recorded spectra reflect the structure of MII.

Figure 8 maps sites with changes in EPR spectra due to photoactivation onto the model discussed above. Although changes in mobility occur at many of the sites, only those with the largest changes, detectable in the reciprocal line width measure (Figure 5, upper panel, dotted line), are shown. Solid and open symbols represent decreased and increased mobility, respectively. Four sites in helix F show large *increases* in mobility (244, 250, 251, 253). These are all immobilized residues that define the tertiary interaction surface of that helix. On the other hand, residues on the exposed face show little or no change, suggesting that the secondary structure is unchanged. Taken together, these results point to a rigid body motion of this helix upon rhodopsin photoactivation that results in a decreased interaction with its neighbors in the vicinity of these residues.

In contrast to helix F, helix E contains only a single residue, 227, that shows a large change on rhodopsin photoactivation, and that reflects a *decrease* rather than an increase in mobility. Residue 231, adjacent to 227 in the helix, shows a smaller decrease in mobility. In the model (Figure 6) these residues are near the contact face with helix F and could be immobilized by a movement of helix F to increase the tertiary interaction with these residues.

The above spectral changes reflect a change in the structure in the protein, presumably accompanying the formation of a MII state (Resek et al., 1993). Structure changes should also result in changes in $\Pi(O_2)$ and Π(NiEDDA). Unfortunately, steady-state changes in collision frequencies are not reliable since the initial MII-like state formed in DM decays on a time scale of minutes, and power saturation measurements require a time long compared to the decay.

Summary and General Conclusions

In summary, the primary conclusions of this work are as follows: (1) the site-directed spin-labeling results in the region of the cytoplasmic membrane/solution interface are consistent with the structural model proposed by Unger and Schertler (1995); (2) the aqueous-exposed E−F interhelical loop likely consists of approximately 1.5 and 3 turn extensions of the E and F helices, respectively, with a turn involving residues 238 and 239; (3) the helical extensions are dynamic, particularly that of helix E, and they are likely optimized for function rather than structural stability; (4) residues 226, 229, 230, 233, and 234, required for transducin

activation (Yang et al., 1996), are located on one face of the E helix, facing inward toward the center of the molecule; (5) large light-dependent changes are observed on the tertiary contact face of the F helix, but not on the exposed face, suggesting a rigid body motion of that helix, and (6) the evidence to date suggests little or no movement of helix E after photoactivation, but that the tertiary interaction of the surface near residue 227 increases as a result of motion of helix F.

Earlier work indicated a smaller but definite motion in helix C (Farahbakhash et al., 1995). Thus, of the helices investigated by site-directed spin-labeling (C, D, E, and F), motion is apparently localized in C and F, with the largest movements seen in the F helix. It is noteworthy that these two helices are those in contact with the ionone ring of retinal (Nakayama & Khorana, 1990, 1991; Nakanishi et al., 1995). Upon photoactivation, isomerization of the chromophore to the *all-trans* configuration is complete within 200 fs (Wang et al., 1994). This isomerization presumably introduces a packing defect (strain) in the hydrophobic core of the protein which relaxes during the MI to MII transition. Our data suggests that the relaxation involves the rigid body rearrangement of at least the C and F helices to repack the core. It may be speculated that rotation of the ionone ring, located between these helices, dictates the motion of these particular helices. Another event, the loss of the salt bridge between the protonated Schiff base linkage to 296 and the counter ion at 113, may be related to the motion in helix C. Indeed, Oprian and co-workers have provided extensive evidence that the presence of this salt bridge is an important structural determinant of the opsin inactive state (Cohen et al., 1992; Zhukovsky et al., 1992; Robinson et al., 1992; Rao et al., 1994). Concerted motion of these, and perhaps other, helices would present new surfaces for interaction with transducin, which could directly interact with the critical residues aligned along the inner face of helix E.

REFERENCES

Altenbach, C., Flitsch, S., Khorana, H. G., Hubbell, W. L. (1989) *Biochemistry 28*, 7806−7812.

Altenbach, C., Marti, T., Khorana, H. G., Hubbell, W. L. (1990) *Science 248*, 1088−1092.

Altenbach, C,. Steinhoff, H-J., Greenhalgh, D. A., Khorana, H. G., & Hubbell, W. L. (1994a*) Biophys. J. 66*, A40.

Altenbach, C., Greenhalgh, D. A., Khorana, H. G., & Hubbell, W. L. (1994b) *Proc. Natl. Acad. Sci. U.S.A. 91*, 1667−1671.

Baldwin, J. M. (1993) *EMBO J. 12*, 1693−1703.

Cohen, G. B., Oprian, D. D., Robinson, P. R. (1992) *Biochemistry 31*, 12592−601.

Farahbakhsh, Z. T., Altenbach, C., & Hubbell, W. L. (1992) *Photochem. Photobiol. 56*, 1091−1033.

Farahbakhsh, Z. T., Hideg, K., & Hubbell, W. L. (1993) *Science 262*, 1416−1419.

Farahbakhsh, Z. T., Huang, Q.-L., Ding, L.-L., Altenbach, C., Steinhoff, H.-J., Horwitz, J., & Hubbell, W. L. (1995a) *Biochemistry 34*, 509−516.

Farahbakhsh, Z. T., Ridge, K. D., Khorana, H. G., & Hubbell, W. L. (1995b) *Biochemistry* 34, 8812−8819.

Farrens, D. L., & Khorana H. G. (1995) *J. Biol. Chem. 270*, 5073−5076.

Freed, J. H. (1976) *Spin-Labeling Theory and Applications* (Berliner, L. J., Ed.) Academic Press, pp 53−132, New York.

Gerstein M., Lesk A. M., & Chothia C. (1994) *Biochemistry 33*, 6739−6749.

Goldman, S. A., Bruno, G. V., & Freed, J. H. (1972) *J. Chem. Phys. 59*, 3071−3091.

Greenhalgh, D., Altenbach, C., Hubbell, W. L., & Khorana, H. G. (1991) *Proc. Natl. Acad. Sci. U.S.A. 88*, 8626−8630.

Hubbell, W. L., & Altenbach, C. (1994) *Curr. Opin. Struct. Biol. 4*, 566−573.

Hubbell, W. L., Froncisz, W., & Hyde, J. S. (1987) *Rev. Sci. Instrum. 58*, 1879−1886.

Karnik S. S., & Khorana H. G. (1990) *J. Biol. Chem. 265*, 17520−17524.

Knudsen, P., & Hubbell, W. L. (1978) *Membr. Biochem*. 1, 297−322.

Konig, B., Arendt, A., McDowell, J. H., Kahlert, M., Hargrave, P. A., & Hofmann, K. P., (1989) *Proc. Natl. Acad. Sci. U.S.A. 86*, 6878−6882.

Mchaourab, H. S., Lietzow, M. A., Hideg, K., & Hubbell, W. L. (1996) *Biochemistry 35*, 7692−7704.

Nakanishi, K., Zhang, H., Lerro, K. A., Takekuma, S., Yamamoto, T., Lien, T. H., Sastry, L., Baek, D. J., Moquin-Pattey, C., Boehm, M. F., et al. (1995) *Biophys. Chem. 56*, 13−22.

Nakayama, T. A., & Khorana, H. G. (1990) *J. Biol. Chem. 265*, 15762−9.

Nakayama, T. A., & Khorana. H. G. (1991) *J. Biol. Chem. 266*, 4269−75.

Pistorius, A. M. A., & de Grip, W. J. (1994) *Biochem. Biophys. Res. Commun. 198*, 1040−1045.

Rao, V. R., Cohen, G. B., & Oprian. D. D. (1994) *Nature 367*, 639−42.

Resek, J. F., Farahbakhsh, Z. T., Hubbell, W. L., & Khorana, H. G. (1993) *Biochemistry 32*, 12025−32.

Robinson, P. R., Cohen, G. B., Zhukovsky, E. A., & Oprian, D. D. (1992) *Neuron 9*, 719−25.

Schertler, G. F., Villa, C., & Henderson, R. (1993) *Nature 362*, 770−772.

Shin, Y.-K., Levinthal, C., Levinthal, F., & Hubbell, W. L. (1993) *Science 259*, 960−963.

Steinhoff, H.-J., Mollaaghababa, R., Altenbach, C., Hideg, K., Krebs, M., Khorana, H. G., & Hubbell, W. L. (1994) *Science 266*, 105−107.

Subramaniam, S., Gerstein, M., Oesterhelt, D., & Henderson, R. (1993) *EMBO J. 12*, 1−8.

Todd, A. P., Cong, J., Levinthal, F., Levinthal, C., & Hubbell, W. L. (1989) *Proteins 6*, 294−305.

Unger, V. M., & Schertler, G. F. (1995) *Biophys. J. 68*, 1776−1786.

Wang, Q., Schoenlein, R. W., Peteanu, L. A., Mathies, R. A., Shank, C. V. (1994) *Science 266*, 422−424.

Yang, K., Farrens, D. L., Hubbell, W. L., & Khorana, H. G. (1996) *Biochemistry 35*, 12464−12469.

Yeagle, P. L., Alderfer, J. L., & Albert, A. D. (1995) *Biochemistry 34*, 14621−14625.

Zhan, H., Oh, K. J., Shin, Y.-K., Hubbell, W. L., & Collier, R. J. (1995) *Biochemistry 34*, 4856−63.

Zhukovsky, E. A., Robinson, P. R., & Oprian, D. D. (1992) *Biochemistry 31*, 10400−5.

BI960849L